Since January 2020 Elsevier has created a COVID-19 resource centre with free information in English and Mandarin on the novel coronavirus COVID-19. The COVID-19 resource centre is hosted on Elsevier Connect, the company's public news and information website.

Science of the Total Environment 755 (2021) 142588

Contents lists available at ScienceDirect

Science of the Total Environment

journal homepage: www.elsevier.com/locate/scitotenv

Different inactivation behaviors and mechanisms of representative pathogens (*Escherichia coli* bacteria, human adenoviruses and *Bacillus subtilis* spores) in g-C_3N_4-based metal-free visible-light-enabled photocatalytic disinfection

Chi Zhang [a], Yi Li [b,*], Chao Wang [c,**], Xinyi Zheng [b]

[a] College of Mechanics and Materials, Hohai University, Xikang Road #1, Nanjing 210098, PR China
[b] Key Laboratory of Integrated Regulation and Resource Development of Shallow Lakes, Ministry of Education, College of Environment, Hohai University, Xikang Road #1, Nanjing 210098, PR China
[c] School of Environmental Science and Engineering, Southern University of Science and Technology, Xueyuan Road #1088, Shenzhen 518055, PR China

HIGHLIGHTS

- Antimicrobial behaviors were comparatively studied by g-C_3N_4/Vis with H_2O_2 and PMS.
- Roles of ROS were quite different depending on both types of oxidants and pathogens.
- Disinfection efficiency could be effectively improved by statistical optimization.
- Selection of added oxidants was determined by the target pathogen and water matrix.

GRAPHICAL ABSTRACT

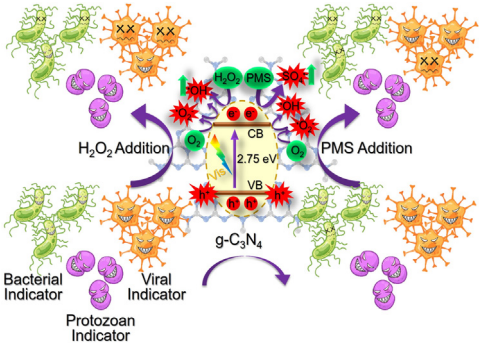

ARTICLE INFO

Article history:
Received 7 August 2020
Received in revised form 13 September 2020
Accepted 21 September 2020
Available online 30 September 2020

Editor: Paola Verlicchi

Keywords:
Carbon nitride
Oxidant addition
Comparative analysis
Disinfection behaviors
Inactivation mechanisms

ABSTRACT

Continuous economic loss and even human death caused by various microbial pathogens in drinking water call for the development of water disinfection systems with the features of environmentally friendly nature, high inactivation efficacy without pathogen regrowth, facile disinfection operation and low energy consumption. Alternatively, g-C_3N_4-based visible-light-enabled photocatalytic disinfection can meet the above requirements and thus has attracted increasing interest in recent years. Here, we explored for the first time the antimicrobial ability and mechanisms of a wide spectrum of representative pathogens ranging from bacteria (*Escherichia coli*), to viruses (human adenoviruses) and spores (*Bacillus subtilis* spores) by g-C_3N_4/Vis system with the assistance of two common oxidants (H_2O_2 and PMS), especially in a comparative perspective. Pristine g-C_3N_4 could achieve a complete inactivation of bacteria (5-log) within 150 min, but displayed negligible antimicrobial activity against human viruses and spores (< 0.5-log). Fortunately, simple addition of oxidants into the system could greatly enhance the inactivation of bacteria (5-log with PMS within 120 min) and human viruses (2.6-log with H_2O_2 within 150 min). Roles of reactive oxygen species were found to be quite different in the disinfection processes, depending on both types of chemical oxidants and microbial pathogens. Additionally, disinfection efficiency could be facilely and effectively improved by statistical optimization of two important operating factors (i.e., catalyst loading

* Correspondence to: Y. Li, College of Environment, Hohai University, Xikang Road #1, Nanjing 210098, PR China.
** Corresponding author.
E-mail addresses: envly@hhu.edu.cn (Y. Li), wangchaoshirley@sustech.edu.cn (C. Wang).

https://doi.org/10.1016/j.scitotenv.2020.142588

and oxidant addition). Selection of added oxidants was determined by not only the target pathogen but also the water matrix. As a proof of concept, this work can provide some meaningful and useful information for advancing the field of green and sustainable water disinfection.

1. Introduction

The war between humans and pathogens has never been stopped over the past thousands of years and seems to continue endlessly, due to the fact that pathogenic microorganisms are ubiquitous in environment and can cause various infectious diseases and even mass death, such as the current COVID-19 pandemic (Baum et al., 2020). Waterborne infectious diseases (e.g., diarrhoea, cholera, dysentery, typhoid, and polio) are generally associated with bacteria, viruses, protozoa and other microbes transmitted via water, and remain a global public health issue as a major source of morbidity and mortality in the world today (Fenwick, 2006; Leclerc et al., 2002; Semenza, 2020; Wang et al., 2019). According to a recent report from WHO (2019), diarrhoea alone is estimated to kill 829,000 people per year, including 485,000 deaths caused by contaminated drinking water with rotavirus and *Escherichia coli*. It is clear to see that a significant proportion of waterborne diseases can be prevented through a safe drinking water supply. Therefore, there is a pressing need to effectively control microbial contamination in drinking water for human health.

Current traditional water disinfection methods including chlorination, ozonation and UV irradiation have raised concerns about the formation of potentially carcinogenic disinfection byproducts (e.g., trihalomethanes, haloacetic acids, bromate, and many others) (Krasner et al., 2006), pathogen reactivation (Li et al., 2017b), and excessive energy consumption (Chen et al., 2017). With an emphasis on sustainable development, photocatalytic water disinfection has become a promising disinfection alternative with the attractive features of little-to-no production of disinfection byproducts, possible complete inactivation of microbial pathogens and potential utilization of renewable solar energy (Fernandez-Ibanez et al., 2020; Liu et al., 2016; Zhang et al., 2019a). In particular, metal-free visible-light-enabled photocatalytic water disinfection has a high solar light-harvesting capability while at the same time avoids the risk of metal leaching into the treated water (Li et al., 2017a; Yadav et al., 2019). Specifically, g-C_3N_4 is rapidly emerging as an easily available and metal-free photocatalyst for various applications in both energy conversion and environmental purification (Liu et al., 2015; Ong et al., 2016), since it was first found to have the ability to split water and generate hydrogen under visible light irradiation (Wang et al., 2009). More recently, g-C_3N_4 has been identified with antimicrobial activity against bacteria (e.g. *Escherichia coli* and *Staphylococcus aureus*) (Huang et al., 2014; Orooji et al., 2020), viruses (e.g. MS2 bacteriophages and human adenoviruses) (Li et al., 2016; Zhang et al., 2019c), and spores (e.g. *Bacillus anthracis* endospores) (Thurston et al., 2017) via the attack of photogenerated reactive oxidative species (ROS), attracting increasing interest as a low cost and environmentally friendly antimicrobial agent candidate for next-generation sustainable water disinfection.

Notably, several basic but important issues on g-C_3N_4-based metal-free visible-light-enabled photocatalytic disinfection need to be addressed before it can be expected to be widely applied in water treatment. Although a number of studies have evaluated the antimicrobial effect of the g-C_3N_4/Vis process, most of them only used a single microorganism under different experimental conditions (Kumar et al., 2020; Zhao et al., 2014). In addition, most have been devoted to the inactivation of bacteria, whereas less have been dedicated to the inactivation of other common pathogens such as viruses and spores (Zhang et al., 2019b). To the best of our knowledge, there is no comprehensive comparative study on the antimicrobial performance of the g-C_3N_4/Vis process for a broad spectrum of pathogens, involving bacteria, human viruses, and spores. Also, a major issue in g-C_3N_4-based metal-free visible-light-enabled photocatalytic disinfection is its slow microbial inactivation kinetics due to the limited photocatalytic activity of pure g-C_3N_4 and the strong environmental resistance of many pathogens (e.g., human adenoviruses and bacterial spores) (Thurston et al., 2017; Zhang et al., 2020; Zhang et al., 2019c). As a result, extensive efforts have been made to modify g-C_3N_4 materials for enhanced photocatalytic disinfection performance (Wang et al., 2013; Xia et al., 2020). Compared to modification of g-C_3N_4 materials with additional processing steps and/or associated reagents, direct addition of commercially available oxidants (e.g., hydrogen peroxide (H_2O_2) and peroxymonosulfate (PMS)) during photocatalysis has been proved to be a simple and efficient approach to improve the degradation efficiency of chemical pollutants (Cui et al., 2012; Tao et al., 2015), whose resistance to disinfection treatment is quite different from microbial pathogens (Marugan et al., 2010; Zhang et al., 2018a). However, to date, neither inactivation behaviors nor mechanisms of these common pathogens in the g-C_3N_4/Vis process with the assistance of oxidants are known, especially in a comparative view.

Taking in consideration the above knowledge gaps and issues in g-C_3N_4-based metal-free visible-light-enabled photocatalytic disinfection, the aim of this work is to i) test the microbicidal capacity of the g-C_3N_4/Vis process on a broad spectrum of representative pathogens (i.e., *Escherichia coli* bacteria, human adenoviruses and *Bacillus subtilis* spores), ii) comparatively evaluate the enhanced disinfection performance of the g-C_3N_4/Vis process with individual addition of two different oxidants (i.e., $^{\bullet}OH$-based H_2O_2 oxidation and $SO_4^{\bullet-}$-based PMS oxidation), iii) explore the corresponding microbial inactivation mechanisms, which might be varied depending on the types of chemical oxidants and microbial pathogens, and iv) statistically optimize the composite disinfection process and attempt at its practicality in drinking water matrices.

2. Experimental

2.1. Representative pathogen surrogates

Escherichia coli bacteria (ATCC 15597) were cultured and propagated in liquid nutrient medium, which contained 10 g of tryptone, 8 g of NaCl, 1 g of glucose, 1 g of yeast extract, 294 mg of $CaCl_2$, 10 mg of thiamine and 1000 mL of deionized water. Briefly, bacterial cultures were incubated at 37 °C for 24 h, and then centrifuged at 3000 rpm for 10 min. The resulting pellet was washed with phosphate-buffered solution (PBS), and ultimately stored at 4 °C before use. Bacterial titer was determined by the spread plate method using solid nutrient medium (15 g of agar), and expressed as colony forming units (CFU)/mL.

Human adenoviruses (type 2, ATCC VR-846) were cultured and propagated in human lung cell line (A549, ATCC CCL-185) and Ham's F-12 K medium, which was supplemented with extra 10% fetal bovine serum and 1% antibiotics. Briefly, lung cell cultures were incubated at 37 °C in humidified air with 5% CO_2 until the cells reached a confluence of 70–80%. Pre-warmed viral cultures were then added into the cellular monolayer, and the mixture was shaken for 45 min to allow sufficient contact between viruses and cells. After 4-day incubation at 37 °C, the infected cells were collected and freeze-thawed three times to release viruses. The mixture was then centrifuged at 1000*g* for 10 min and the supernatant was filtered through a 0.45 μm membrane for virus

purification. The resulting filtrate was concentrated and washed with PBS, and ultimately stored at −80 °C before use. Virus titer was measured by the most probable number (MPN) method using 96-well plate, and expressed as MPN/mL.

Bacillus subtilis spores (ATCC 6633) were prepared from the corresponding strain in liquid broth medium. The culture procedures of *Bacillus subtilis* were similar to the above described for *Escherichia coli*. The difference is that *Bacillus subtilis* was next inoculated and incubated on solid medium with 10-fold dilutions of nutrients to induce sporulation. *Bacillus subtilis* spores were collected by rinsing with PBS, and then centrifuged at 3000 rpm for 10 min. The resulting pellet was washed and resuspended in PBS, but needed to be heated at 80 °C for 20 min to kill any remaining vegetative cells before use. Spore titer was detected by the spread plate method using solid nutrient medium, and also expressed as CFU/mL.

2.2. g-C_3N_4-based photocatalytic disinfection

The g-C_3N_4 visible-light-photocatalysts were obtained by directly heating low-cost melamine as a sole precursor in covered crucibles using muffle furnace according to the pioneering study of Yan et al. (2009), and well characterized in our previous studies (Li et al., 2016; Zhang et al., 2018b). All microbial stock solutions were diluted into 20 mL of deionized water in 50-mL beakers to prepare the individual microbial suspensions with an initial concentration of 10^5 CFU/mL or MPN/mL. Then a certain dose of the freshly prepared g-C_3N_4 photocatalysts and the oxidants (H_2O_2 or PMS) were added for microbial inactivation with continuous stirring at room temperature. The light source was a 300 W Xenon lamp with a cutoff filter to provide visible light irradiation (≥ 400 nm, 150 mW/cm^2). Before illumination, the system was first kept in the dark for 30 min to reach adsorption-desorption equilibrium between photocatalysts and microorganisms. Microbial samples were taken at time intervals of 0, 30, 60, 90, 120 and 150 min during photocatalytic disinfection, and were immediately counted to avoid further inactivation. Microbial solutions without g-C_3N_4 photocatalysts were irradiated under the same experimental conditions as light control, and microbial suspensions with g-C_3N_4 photocatalysts but without visible light irradiation was used as dark control. The microbial inactivation efficiency was calculated as log [C_t/C_0], where C_0 and C_t were the microbial titer before and after photocatalytic disinfection, respectively.

2.3. ROS detection

A series of photocatalytic disinfection experiments were carried out in the presence of various individual scavengers to selectively quench the photogenerated ROS to elucidate the microbial inactivation mechanisms of g-C_3N_4-based metal-free visible-light-enabled photocatalytic disinfection for different types of pathogens. The used scavengers were selected as oxalate (0.5 mM) for photogenerated holes (h^+), Cr (VI) (0.05 mM) for photogenerated electrons (e^-), Fe(II) (1.5 mM) for H_2O_2, methanol (10 mM) for both $^{\bullet}OH$ and $SO_4^{\bullet-}$, TBA (10 mM) for $^{\bullet}OH$, TEMPOL (1 mM) for $^{\bullet}O_2^-$, and L-histidine (0.5 mM) for $^1O_2$, respectively, in order to exert the maximum scavenging effect but without toxicity to the target microbial pathogens (Rodríguez-Chueca et al., 2020; Zhang et al., 2018a; Zhang et al., 2019c). Moreover, electron spin resonance spectroscopy (ESR) was performed for further verification of $^{\bullet}OH$ and $SO_4^{\bullet-}$ generation on a Bruker EMXplus spectrometer using 5,5-dimethyl-1-pyrroline N-oxide (DMPO) as the spin trapping agents.

2.4. Microbial morphology damage observation

Bacterial samples were fixed by 2.5% glutaraldehyde, washed by PBS three times, and gradually dehydrated by ethanol series from 30% to 100%, followed by freeze-drying and gold-coating, for morphology observation by a SU8010 scanning electron microscope (SEM, Hitachi, Japan). In addition to fixation and washing procedures, viral samples were required to be negatively stained with 2% uranyl acetate for morphology observation by a FEI Talos F200X transmission electron microscope (TEM, Thermo Fisher Scientific, USA).

2.5. Process optimization design and statistical analysis

The two important operating parameters in g-C_3N_4-based metal-free visible-light-enabled photocatalytic disinfection, namely catalyst loading (X_1, g/L) and oxidant addition (X_2, mM), were interactively analyzed and optimized using response surface methodology (RSM) as a powerful statistical tool. The photocatalytic inactivation of bacteria (Y_1) and viruses (Y_2) after 60 and 120 min of visible light irradiation was set as the responses (log [C_t/C_0]), respectively. Central composite design (CCD) as an efficient and flexible statistical experimental design method was utilized to evaluate the interaction effect of these two variables on the inactivation responses based on a set of 13 sub-experiments. And the corresponding designed ranges and levels of independent variables in CCD are presented in Table S1. The obtained experimental results were fitted to a quadratic polynomial model:

$$Y = \beta_0 + \sum_{i=1}^{k} \beta_i X_i + \sum_{i=1}^{k} \beta_{ii} X_i^2 + \sum_{1 \le i < j}^{k} \beta_{ij} X_i X_j \quad (1)$$

where Y is the predicted response, β_0 is the constant, βi, βii, and βij are the linear, squared, and interaction coefficients, respectively. And k is the number of variables in the model (here k = 2). All statistical assessments, including analysis of variance (ANOVA), were conducted using Design-Expert® software (version 8.0.6.1).

3. Results and discussion

To systematically evaluate the antimicrobial potency and efficacy of g-C_3N_4-based metal-free visible-light-enabled photocatalytic disinfection, *Escherichia coli*, human adenoviruses, and *Bacillus Subtilis* spores were chosen as microbial representatives of pathogenic bacteria, viruses, and protozoa, respectively (Sun et al., 2016). In detail, *Escherichia coli* is the most commonly used and accepted indicator bacteria in photocatalytic disinfection processes, due to the prevalent occurrence in environment and the easy cultivation in lab. Human adenoviruses have been employed here when considering the controversy over the suitability of bacteriophages as surrogates for human viruses in water treatment processes. And *Bacillus subtilis* spores have been tested because of their high resistance to various disinfection treatments, including heat, UV radiation, and even chlorination.

3.1. Microbial inactivation behaviors

3.1.1. Can g-C_3N_4 be a universal antimicrobial weapon?

The quite different microbial inactivation behaviors ranging from bacteria to human viruses and spores in the g-C_3N_4/Vis system have been clearly observed in Fig. 1. As seen in the light and dark control groups, neither visible-light photolysis nor g-C_3N_4 materials in dark could induce any inactivation of these microorganisms. The results suggest that, on one hand, most microbial pathogens are stable and can even proliferate under visible light irradiation without photocatalysts, on the other hand, the g-C_3N_4 material alone is biocompatible in the dark and exert low or no toxicity to microorganisms in water. When the light was turned on in the presence of g-C_3N_4, all *Escherichia coli* bacteria (5-log) were inactivated within 150 min (Fig. 1a), declaring a good bactericidal effect induced by the g-C_3N_4/Vis system. Unfortunately, almost no human adenoviruses (Fig. 1b) and *Bacillus subtilis* spores (Fig. 1c) were inactivated during the same process. Compared to common bacteria with fragile cell membranes, human viruses have highly

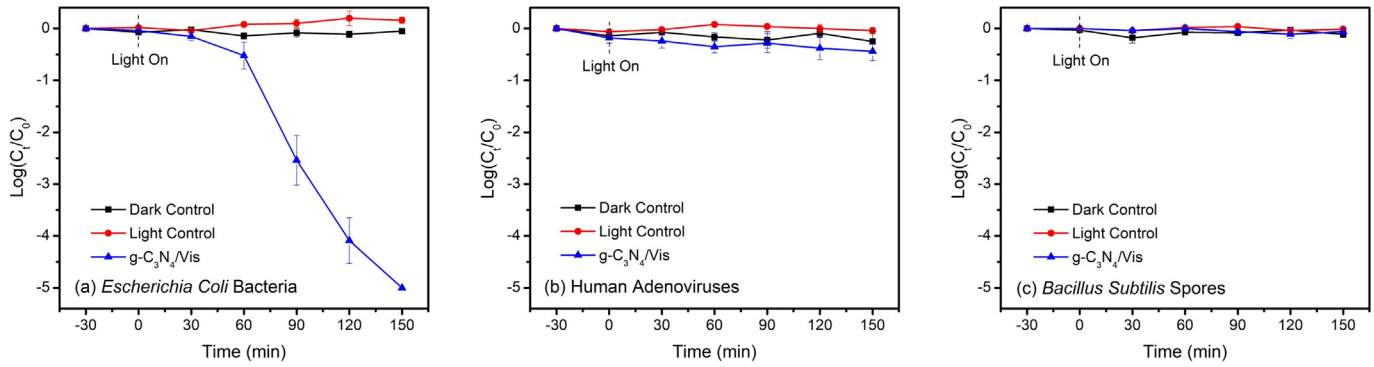

Fig. 1. Inactivation behaviors of representative pathogens in g-C_3N_4-based metal-free visible-light-enabled photocatalytic disinfection: (a) *Escherichia coli* bacteria, (b) human adenoviruses, and (c) *Bacillus subtilis* spores. Experimental conditions: $[catalyst]_0 = 0.1$ g/L.

rigid protein shells and bacterial spores have extremely thick cell walls, which can protect them well from a wide range of harsh environments, including chemical disinfectants, UV irradiation, and photocatalytic treatment (Płonka and Pieczykolan, 2020; Sun et al., 2016; Zhang et al., 2019b). This is to say that g-C_3N_4 can be served as a powerful antimicrobial weapon against bacteria rather than human viruses, protozoa, and not to mention other resistant pathogens with complex biological compositions and structures.

3.2. Oxidant addition effects

3.2.1. Which antimicrobial accelerator is better: H_2O_2 or PMS?

As well known, H_2O_2 is one of the most commonly used oxidants for enhanced water treatment, owing to its low-cost and green nature. Alternatively, PMS has also received increasing attention as a stable solid oxidant with the additional advantage of convenient storage and transportation. Notably, $^{\bullet}$OH-based H_2O_2 oxidation (Eo $^{\bullet}OH+H^+/H_2O = 2.73$ V) and $SO_4^{\bullet-}$-based PMS oxidation (Eo $SO_4^{\bullet-}/SO_4^{2-} = 2.43$ V) have a similar redox potential to participate in a variety of reactions with inorganic and organic molecules (Gligorovski et al., 2015). Both of them have been confirmed to effectively improve the photocatalytic degradation activity of g-C_3N_4 towards many chemical pollutants (Cui et al., 2012; Tao et al., 2015). However, their enhancing effects on the photocatalytic disinfection activity of g-C_3N_4 towards various microbial pathogens are still needed to be systematically studied and comparatively analyzed.

The viability of representative pathogens used in this study was found to be unaffected in the presence of H_2O_2 or PMS alone at a low concentration (0.5 mM) under visible light irradiation. Expectedly, addition of H_2O_2 or PMS into the g-C_3N_4/Vis system can accelerate and promote microbial inactivation, although in different degrees (Fig. 2). For bacterial indicators, a complete inactivation of *Escherichia coli* (5-log) was quickly achieved within 120 min with the addition of either H_2O_2 or PMS, reducing the disinfection time by 20% (Fig. 2a). For viral indicators, a partial inactivation of human adenoviruses could be observed within 150 min, namely ~2.6-log with H_2O_2 addition and ~1.7-log with PMS addition, respectively (Fig. 2b). The more enhancement in adenovirus inactivation induced by H_2O_2 might be attributed to the higher reaction rate and efficiency between $^{\bullet}$OH radicals and biological proteins, leading to rapid and irreversible modification of viral protein coats (Gau et al., 2010; Rinas et al., 2016). While for protozoan indicators, a very slight inactivation of *Bacillus subtilis* spores (less than 1-log) was obtained only with the addition of H_2O_2 instead of PMS (Fig. 2c). The enhancing effects of addition of H_2O_2 and PMS to the g-C_3N_4/Vis disinfection system are quite different, depending on the types of added oxidants and target microorganisms. On one hand, the added oxidants could assist the g-C_3N_4/Vis system to produce some more specific ROS. Although certain ROS such as $^{\bullet}$OH are able to react unselectively and instantaneously with the surrounding compounds, the redox capacity of ROS towards one compound is closely related to their types and concentrations (Nosaka and Nosaka, 2017). On the other hand, the target microorganisms with diverse biological structures and metabolic activities could have different resistance and response to a specific ROS attack. In view of both disinfection efficiency and operational simplicity, PMS is recommended for bacterial inactivation while H_2O_2 is more preferred for viral inactivation as an effective antimicrobial accelerator in g-C_3N_4-based metal-free visible-light-enabled photocatalytic disinfection. As for some certain pathogens with high resistance such as protozoa, another more powerful antimicrobial agent or approach is required to be further explored.

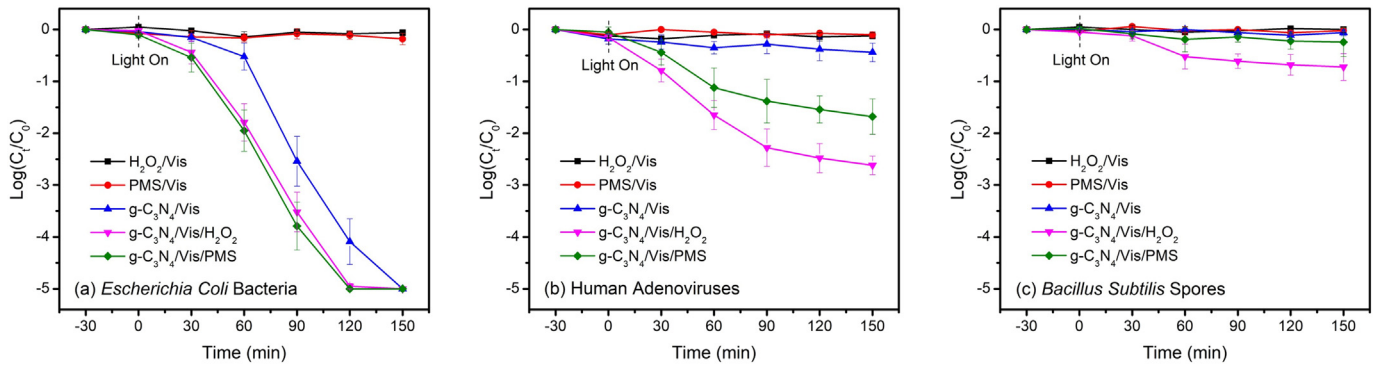

Fig. 2. Inactivation behaviors of representative pathogens in g-C_3N_4-based metal-free visible-light-enabled photocatalytic disinfection with oxidant addition (H_2O_2 versus PMS): (a) *Escherichia coli* bacteria, (b) human adenoviruses, and (c) *Bacillus subtilis* spores. Experimental conditions: $[catalyst]_0 = 0.1$ g/L, $[oxidant]_0 = 0.5$ mM.

3.3. Microbial inactivation mechanisms

3.3.1. Roles of ROS in microbial inactivation: Same or not?

Given that microbial inactivation in photocatalytic disinfection systems is generally induced by ROS via the oxidative attack and damage, a series of scavenging studies have been performed to elucidate the roles of ROS in microbial inactivation (Fig. 3a–d). Conspicuously, the addition of Cr(VI) to quench photogenerated e^- was found to inhibit the microbial inactivation most significantly in all systems, claiming a dominant role of e^- in g-C_3N_4-based metal-free visible-light-enabled photocatalytic disinfection. On one hand, according to the Eqs. (2)–(6), the production of photogenerated ROS is considered from the conduction band (−1.35 V) rather than the valence band (+1.40 V) of g-C_3N_4 materials under thermodynamically favorable conditions. On the other hand, according to the Eqs. (6) and (7), the activation of added oxidants is also considered from a reductive pathway. Moreover, ROS generation has been intuitively confirmed in the ESR spectra (Fig. 3e and f), further verifying the different major ROS in the H_2O_2-assisted (i.e., $^{\bullet}OH$) and PMS-assisted (i.e., $SO_4^{\bullet-}$) g-C_3N_4/Vis systems.

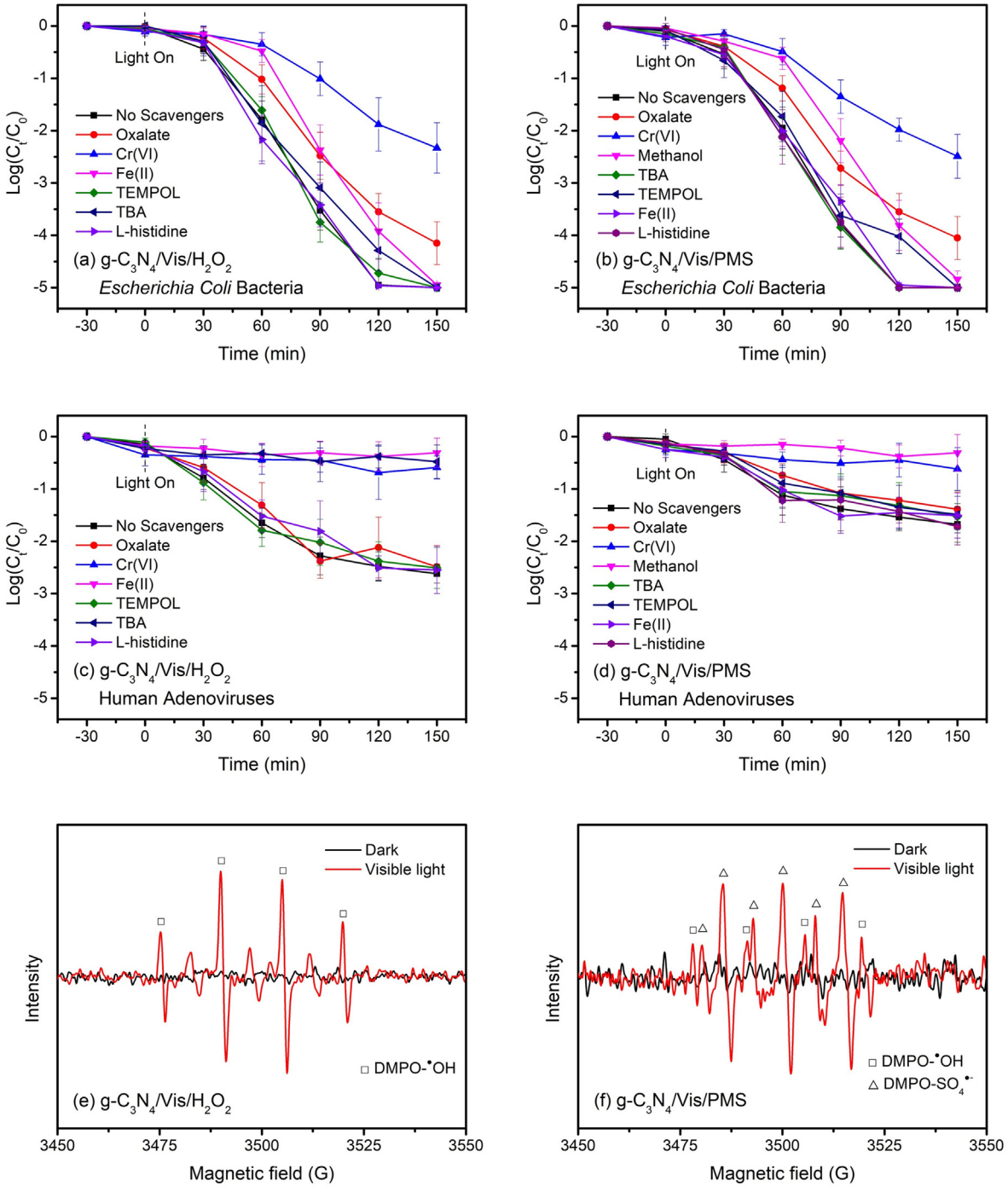

Fig. 3. Inactivation mechanisms of representative pathogens in g-C_3N_4-based metal-free visible-light-enabled photocatalytic disinfection: (a) *Escherichia coli* bacteria in the g-C_3N_4/Vis/H_2O_2 system, (b) *Escherichia coli* bacteria in the g-C_3N_4/Vis/PMS system, (c) human adenoviruses in the g-C_3N_4/Vis/H_2O_2 system, (d) human adenoviruses in the g-C_3N_4/Vis/PMS system, ESR spectra of (e) DMPO-$^{\bullet}OH$ in the g-C_3N_4/Vis/H_2O_2 system and (f) DMPO-$^{\bullet}OH$ and DMPO-$SO_4^{\bullet-}$ in the g-C_3N_4/Vis/PMS system Experimental conditions: $[catalyst]_0$ = 0.1 g/L, $[oxidant]_0$ = 0.5 mM. $[DMPO]_0$ = 100 mM.

$$H_2O + h^+ \rightarrow {}^{\bullet}OH + H^+ \text{ (Eo redox} = +2.38 \text{ V)} \quad (2)$$

$$OH^- + h^+ \rightarrow {}^{\bullet}OH \text{ (Eo redox} = +1.55 \text{ V)} \quad (3)$$

$$O_2 + e^- \rightarrow {}^{\bullet}O_2^- \text{ (Eo redox} = -0.33 \text{ V)} \quad (4)$$

$${}^{\bullet}O_2^- + 2H^+ + e^- \rightarrow H_2O_2 \text{ (Eo redox} = +0.89 \text{ V)} \quad (5)$$

$$H_2O_2 + e^- \rightarrow {}^{\bullet}OH + OH^- \text{ (Eo redox} = +0.38 \text{ V)} \quad (6)$$

$$HSO_5^- + e^- \rightarrow SO_4^{\bullet -} + OH^- \text{ (Eo redox} = +1.19 \text{ V)} \quad (7)$$

In addition, considering that $^1O_2$ as a non-radical ROS is capable of efficiently reacting with a wide range of biomolecules such as nucleic acids, proteins, and lipids, L-histidine as the specific chemical quencher was added in the systems (Di Mascio et al., 2019). However, in contrast, no inhibitory effect was observed on the microbial inactivation in all systems, suggesting a negligible role of $^1O_2$ in g-C_3N_4-based metal-free visible-light-enabled photocatalytic disinfection. This is probably due to the poor yields and selectivity for $^1O_2$ generation from pristine g-C_3N_4 with an insufficient inter-system crossing process (Wang et al., 2016).

For bacterial indicators, the direct oxidative damage from photogenerated h^+ cannot be ignored, based on a moderate inhibition of *Escherichia coli* inactivation with the addition of oxalate in these two systems of g-C_3N_4/Vis/H_2O_2 (Fig. 3a) and g-C_3N_4/Vis/PMS (Fig. 3b). At the same time, bacterial inactivation was almost unaffected in the presence of TEMPOL ($^{\bullet}O_2^-$ scavenger), implying that the remaining h^+ assisted with one-electron reduction of oxidants (either $^{\bullet}OH$ or $SO_4^{\bullet -}$) could still effectively kill bacteria. In the g-C_3N_4/Vis/H_2O_2 system, $^{\bullet}OH$ radicals would be generated from both the multistep reduction of O_2 (Eqs. (3)–(5)) and the one-electron reduction of added H_2O_2 (Eq. (5)). Interestingly, bacterial inactivation was only slightly inhibited with the addition of TBA ($^{\bullet}OH$ scavenger) and Fe(II) (H_2O_2 scavenger), indicating that $^{\bullet}O_2^-$ could play a lethal role in bacterial inactivation. This phenomenon was also observed in the g-C_3N_4/Vis/PMS system with the addition of methanol ($^{\bullet}OH$ and $SO_4^{\bullet -}$ scavenger). As a result, photogenerated h^+, e^- derived ROS, and the added oxidant-activated ROS, including $^{\bullet}O_2^-$, $^{\bullet}OH$ and $SO_4^{\bullet -}$, can all contribute to bacterial inactivation in the g-C_3N_4-based metal-free visible-light-enabled photocatalytic disinfection.

While for viral indicators, the role of photogenerated h^+ seemed to be dispensable in these two systems of g-C_3N_4/Vis/H_2O_2 (Fig. 3c) and g-C_3N_4/Vis/PMS (Fig. 3d), according to little inhibition of human adenovirus inactivation with the addition of oxalate. Another difference from bacterial inactivation is that viral inactivation was greatly inhibited with the addition of TBA in the g-C_3N_4/Vis/H_2O_2 system, signifying that $^{\bullet}OH$ rather than $^{\bullet}O_2^-$ is a dominant lethal factor for viral inactivation. Oppositely, human adenoviruses could be still inactivated with the addition of TBA in the g-C_3N_4/Vis/PMS system, demonstrating that $SO_4^{\bullet -}$ can be another lethal factor for viral inactivation. Given the limited inactivation of human adenoviruses induced by pure g-C_3N_4 alone under visible light irradiation, only the oxidant-activated ROS with high redox potentials (i.e., $^{\bullet}OH$ and $SO_4^{\bullet -}$) can contribute to viral inactivation in g-C_3N_4-based metal-free visible-light-enabled photocatalytic disinfection.

3.3.2. Can g-C_3N_4-based metal-free visible-light-enabled photocatalytic disinfection definitely kill pathogens?

Notably, a unique feature of microbial pathogens, different from chemical compounds, is that they have the ability to self-repair damage under favorable conditions. The microbial regrowth tests of 48-h dark incubation have been conducted and found that neither *Escherichia coli* bacteria nor human adenoviruses could be visualized in culture (Fig. S1), certifying the definite lethal effects of g-C_3N_4-based metal-free visible-light-enabled photocatalytic disinfection with oxidant oxidation towards microbial pathogens. Furthermore, typical SEM images of bacterial cells and TEM images of viral particles have intuitively presented the damage of representative pathogens (Fig. 4). Obviously, the biological structures of *Escherichia coli* bacteria and human adenoviruses were severely destroyed, especially for bacteria, without the

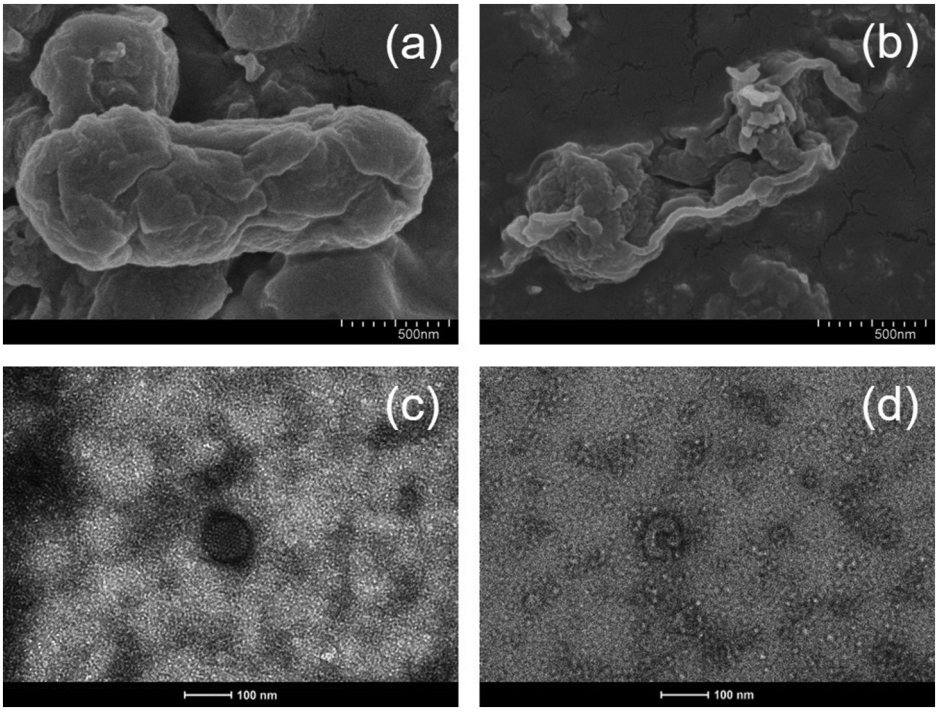

Fig. 4. Representative pathogen damage induced by g-C_3N_4-based metal-free visible-light-enabled photocatalytic disinfection: SEM images of *Escherichia coli* bacteria (a) before and (b) after treatment with PMS addition, and TEM images of human adenoviruses (c) before and (d) after treatment with H_2O_2 addition.

possibility of regeneration after the photocatalytic treatment of g-C_3N_4/Vis/PMS and g-C_3N_4/Vis/H_2O_2, respectively.

3.4. Photocatalytic disinfection process optimizations

3.4.1. Can there be a convenient way to achieve satisfactory disinfection?

The statistical tool RSM has been successfully used for optimizing photocatalytic processes, but mainly involving the degradation of non-living chemical pollutants in which reaction kinetics and mechanisms are quite different from living microbial pathogens. Here, two easy-to-operate but important disinfection parameters (i.e., catalyst loading X_1 and oxidant addition X_2) have been chosen for achieving satisfactory inactivation towards microbial pathogens (Y) in the g-C_3N_4-based photocatalytic disinfection system (Tables S2 and S4). Then, two empirical second order polynomial models were developed for bacterial inactivation in the g-C_3N_4/Vis/PMS system (Eq. (8)) and viral inactivation in the g-C_3N_4/Vis/H_2O_2 system (Eq. (9)), respectively.

$$Y_{bacteria} = +0.30655 - 16.46050X_1 - 0.94100X_2 - 15.90000X_1X_2 + 52.50000{X_1}^2 + 0.52000{X_2}^2 \quad (8)$$

$$Y_{virus} = +1.13687 - 27.23185X_1 - 3.98238X_2 - 17.60000X_1X_2 + 118.12500{X_1}^2 + 3.18500{X_2}^2 \quad (9)$$

Significance and adequacy of the established models were statistically checked by ANOVA (Tables S3 and S5). Both of the models exhibited a high F-value (35.54 and 28.18) along with a low *P*-value (< 0.0001 and 0.0002), implying that they are statistically significant. The lack of fit F-value (4.07 and 3.20) was not significant relative to the pure error, which is good for a model. Again, the predicted R^2 of 0.7823 and 0.7407 was in reasonable agreement with the adjusted R^2 of 0.9350 and 0.9189, respectively. Meanwhile, the adequate precision (20.105 and 15.659) was desirable here (> 4), indicating an adequate signal to noise ratio. All the above results of statistical analysis have strongly suggested that these two constructed models can be successfully used to navigate the design space. This conclusion was further supported by the linear plots in Figs. 5 and 6. On one hand, the predicted values matched well with the actual responses (Figs. 5a and 6a). On the other hand, neither response transformation was required nor apparent problem with normality would occur (Figs. 5b and 6b), all confirming the high accuracy of the established models.

According to the analysis data in Table S3, the terms of X_1, X_2, X_1X_2, and X_1^2 with *P*-values <0.0500 were significant, representing a great contribution to bacterial inactivation response. And the order of contribution was: $X_1 > X_2 > X_1X_2 > X_1^2$, describing a greater contribution of catalyst loading than oxidant addition towards bacterial inactivation in the g-C_3N_4/Vis/PMS system. While according to the analysis data in Table S5, the order of significant contribution was: $X_2 > X_1 > X_1^2 > X_2^2 > X_1X_2$, demonstrating a larger proportion of oxidant addition than catalyst loading towards viral inactivation in the g-C_3N_4/Vis/H_2O_2 system. This opposite trend can be related to a higher sensitivity of *Escherichia coli* bacteria in comparison of human adenoviruses to g-C_3N_4 photocatalysts under visible light irradiation.

Besides, the interaction effect between catalyst loading and oxidant addition (X_1X_2) cannot be neglected, which was further elucidated by 2D contour (Figs. 5c and 6c) and 3D response surface analysis (Figs. 5d and 6d). From an individual viewpoint, the increase of catalyst loading and oxidant addition can enhance the microbial inactivation owing to the increase of surface reaction active sites and ROS for photocatalytic disinfection. However, the further increase of either catalyst

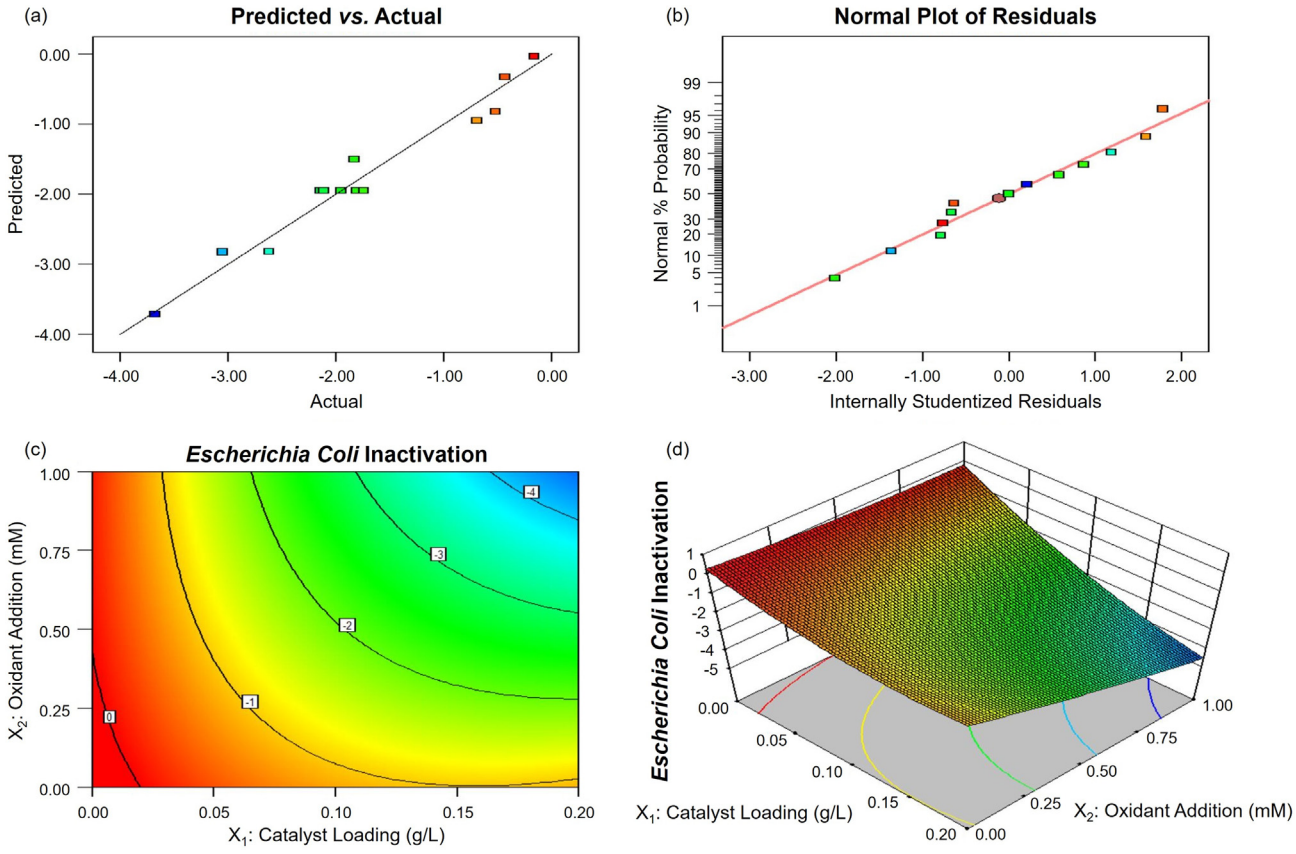

Fig. 5. Optimization plots of g-C_3N_4-based metal-free visible-light-enabled photocatalytic disinfection with PMS addition for bacterial inactivation: (a) predicted versus actual values, (b) normal % probability versus internally studentized residuals, (c) 2D contour and (d) 3D response surface for interaction between catalyst loading (X_1) and oxidant addition (X_2).

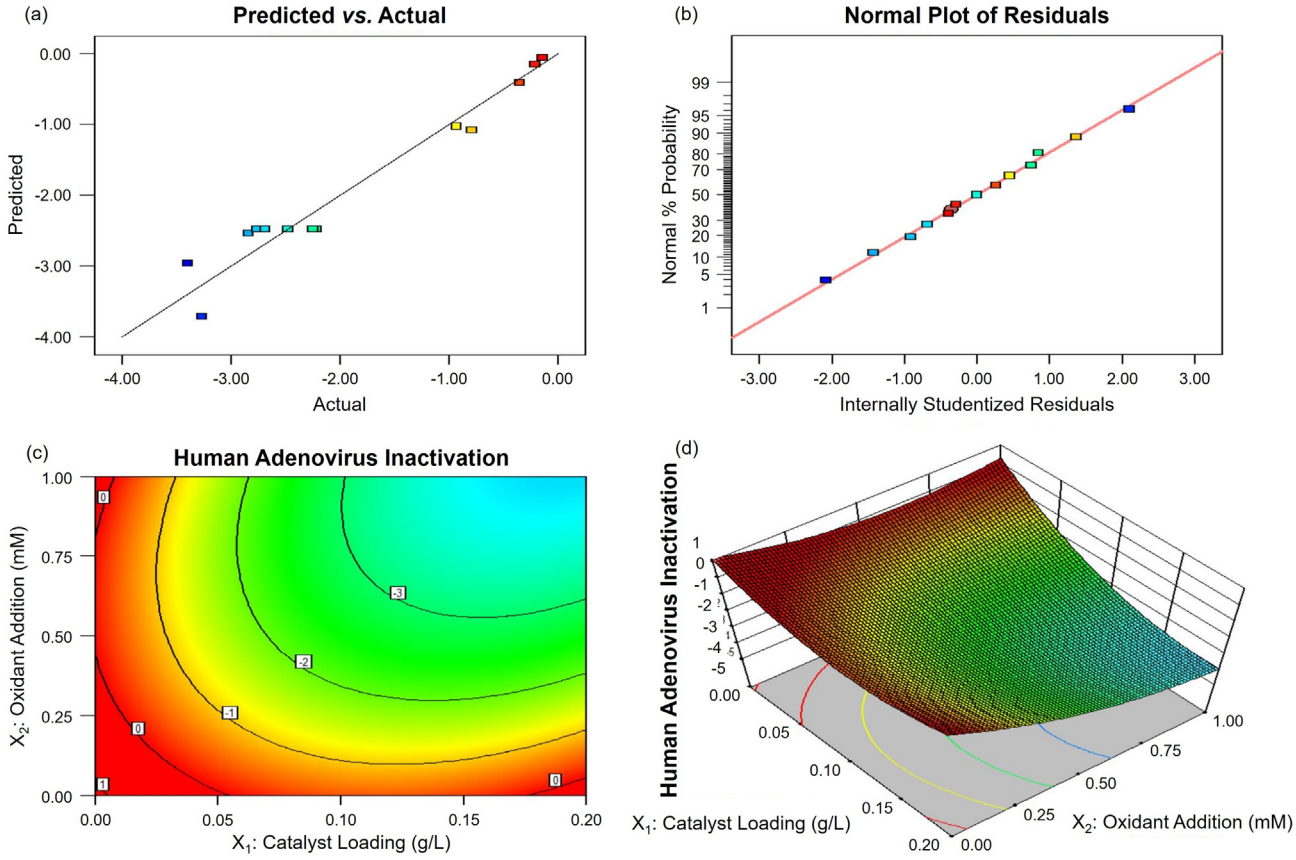

Fig. 6. Optimization plots of g-C_3N_4-based metal-free visible-light-enabled photocatalytic disinfection with H_2O_2 addition for viral inactivation: (a) predicted versus actual values, (b) normal % probability versus internally studentized residuals, (c) 2D contour and (d) 3D response surface for interaction between catalyst loading (X_1) and oxidant addition (X_2).

loading or oxidant addition can slightly deteriorate microbial inactivation because of the shading effect of excess catalyst loading to limit light penetration and the scavenging effect of excess oxidant addition to produce less reactive ROS (Eqs. (10) and (11)). From an interactive viewpoint, the increase of catalyst loading along with oxidant addition provides sufficient active sites for generating photogenerated e^- to capture and activate oxidants (Eqs. (6) and (7)), which can reduce and even eliminate their scavenging effects. The analysis highlights the regulation effectiveness of these two operating parameters, namely catalyst loading and oxidant addition, towards microbial pathogen inactivation in g-C_3N_4-based metal-free visible-light-enabled photocatalytic disinfection.

$$\text{Excess } H_2O_2 + {}^{\bullet}OH \rightarrow {}^{\bullet}O_2H + H_2O \quad (10)$$

$$\text{Excess } HSO_5^- + SO_4^{\bullet-} \rightarrow SO_5^{\bullet-} + SO_4^{2-} + H^+ \quad (11)$$

The optimal solutions were obtained by a numerical optimization method to achieve the best inactivation performance for representative pathogens in g-C_3N_4-based metal-free visible-light-enabled photocatalytic disinfection. The two developed models predicted the maximum bacterial inactivation of 4.49-log at 60 min in the g-C_3N_4/Vis/PMS system with a solution of 0.20 g/L and 1.00 mM for g-C_3N_4 loading and PMS addition, and maximum viral inactivation of 3.91-log at 120 min in the g-C_3N_4/Vis/H_2O_2 system with a solution of 0.19 g/L and 1.00 mM for g-C_3N_4 loading and H_2O_2 addition, respectively. Moreover, the verification and stability experiments have been carried out under the optimized conditions (Fig. 7). The actual bacterial inactivation at 60 min (Fig. 7a) and viral inactivation at 120 min (Fig. 7c) were tested to be ~4.4-log and ~3.8-log, respectively. The actual measurements are very close to the predicted values, identifying the validity of these prediction models. The disinfection ability of g-C_3N_4/Vis/PMS was stable against bacteria (Fig. 7b), while the disinfection ability of g-C_3N_4/Vis/H_2O_2 was slightly but acceptably decreased against human viruses after five cycles (Fig. 7d). After optimization by RSM, the disinfection time for a complete inactivation of *Escherichia coli* bacteria was reduced by 25%, and the disinfection efficiency for inactivation of human adenoviruses was enhanced by 46%, stating a convenient way to achieve satisfactory disinfection.

3.5. Practicality in real water matrices

3.5.1. Flexible selection of the established system in various waters

Considering the environmentally friendly and sustainable features of g-C_3N_4-based metal-free visible-light-enabled photocatalytic disinfection, it is expected to improve drinking water safety and thus tested in tap water and source water samples (Fig. 8). To be satisfactory, a complete inactivation of *Escherichia coli* bacteria was still obtained in tap water by either g-C_3N_4/Vis/H_2O_2 or g-C_3N_4/Vis/PMS (Fig. 8a). However, bacterial inactivation was notably inhibited in source water (Fig. 8b), which might be attributed to the presence of a higher level of dissolved organic matters for occupying active sites and consuming ROS from photocatalysts. An interesting observation was that the g-C_3N_4/Vis/PMS system prominently outperformed the g-C_3N_4/Vis/H_2O_2 system for bacterial inactivation (~5 log versus ~4.5 log) in the relatively complex water matrix (Fig. 8b). This disinfection superiority of g-C_3N_4/Vis/PMS is possibly ascribed to a highly selective reactivity of $SO_4^{\bullet-}$ with the electron-rich moieties on the surface of bacterial cell membranes (Wordofa et al., 2017). Additionally, more than 3-log of human

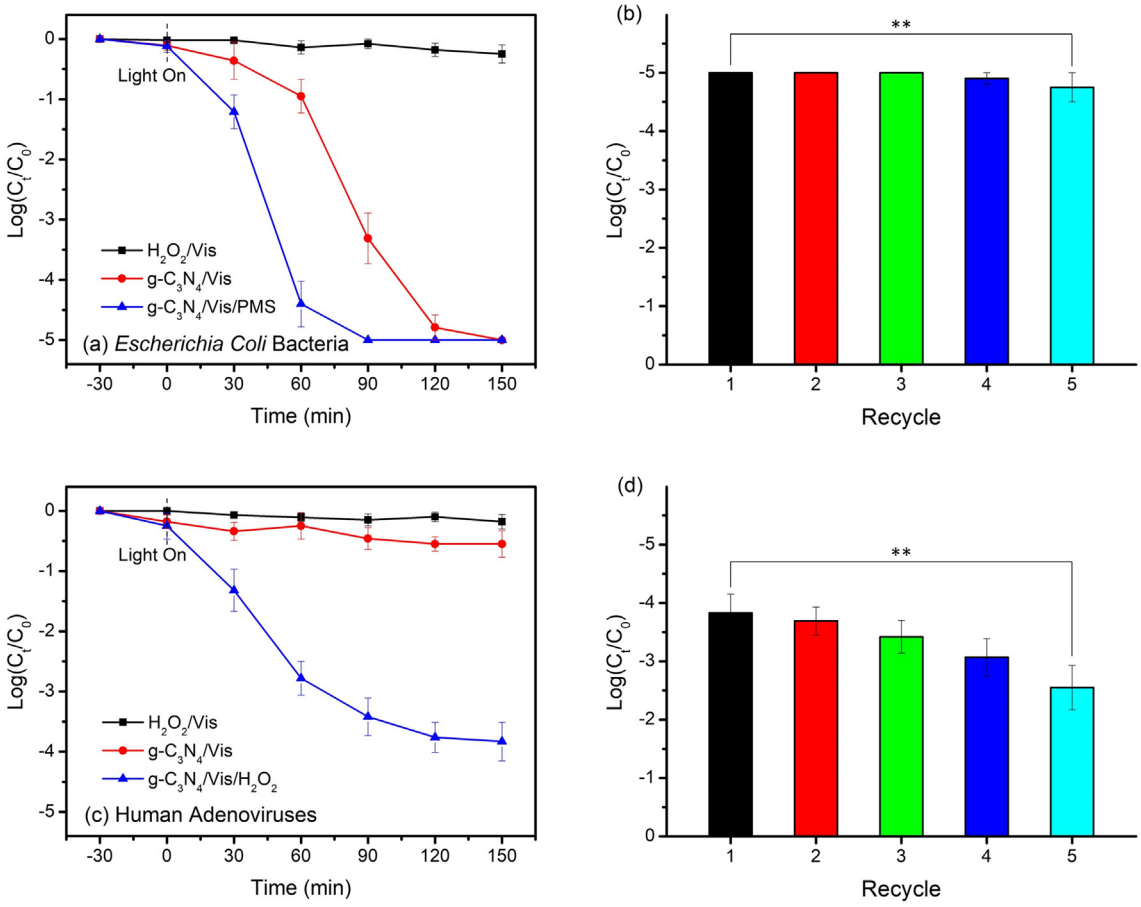

Fig. 7. Photocatalytic disinfection ability and stability of g-C_3N_4-based metal-free visible-light-enabled photocatalytic disinfection under the optimal solution: (a) and (b) *Escherichia coli* bacteria, (c) and (d) human adenoviruses.

adenoviruses was inactivated in tap water (Fig. 8c), whereas only 2-log inactivation was achieved in source water by g-C_3N_4/Vis/H_2O_2 (Fig. 8d), not mention to by g-C_3N_4/Vis/PMS. This requires that the established disinfection system is able to bind to human viruses both effectively and selectively in the complex real water matrices.

Given the difficult recovery of powdered g-C_3N_4 materials from water, the integration of g-C_3N_4 photocatalysis and membrane separation into multifunctional membranes is considered as promising alternatives for practical water disinfection (Castro-Muñoz, 2020; Ursino et al., 2018). In addition to catalyst immobilization and recycling, such membranes can possess not only high chemical and mechanical stability, but also good antimicrobial and antifouling properties driven by renewable solar energy (Castro-Muñoz, 2019; Pichardo-Romero et al., 2020). They are expected to be used in either drinking water treatment plants for centralized water disinfection or solar reactors for point-of-use water disinfection (Castro-Muñoz et al., 2020; Castro-Muñoz et al., 2016). But the development and potential applications of g-C_3N_4-based membrane technologies for water disinfection still need further exploration.

4. Conclusions

In this study, g-C_3N_4-based metal-free visible-light-enabled photocatalytic disinfection with addition of common oxidants (H_2O_2 versus PMS) was comparatively examined against a broad spectrum of representative pathogens, including *Escherichia coli* Bacteria, Human Adenoviruses and *Bacillus subtilis* spores. The major conclusions can be drawn as follows:

- Although the pristine g-C_3N_4 material exhibits a good antibacterial activity towards the bacterial indictors under visible light irradiation, it cannot be a universal antimicrobial weapon due to a very limited disinfection activity against the viral and protozoan indicators.
- Simple addition of common low-cost oxidants can significantly enhance the disinfection efficiency and efficacy of the g-C_3N_4/Vis system against bacteria and human viruses, while inactivation of some highly resistant pathogens (e.g., bacterial spores and protozoa) is still a challenge.
- Considering both disinfection efficiency and operational simplicity, PMS is recommended for bacterial inactivation while H_2O_2 is preferred for viral inactivation as an antimicrobial accelerator. The inactivation mechanisms are dependent on the types of added oxidants and target pathogens.
- Disinfection efficiency of g-C_3N_4/Vis/H_2O_2 and g-C_3N_4/Vis/PMS can be effectively improved through facile adjustment of catalyst loading and oxidant addition by RSM. Selection of these disinfection systems is flexible, based on the type of target pathogens and the matrix of water samples.

Last but not least, the potential applications of g-C_3N_4-based metal-free visible-light-enabled photocatalytic disinfection are recommended to be combined with other mature technologies such as membrane separation. Such combinations are believed to achieve multifunctional water remediation, including not only the inactivation of microbial pathogens but also the removal and even recovery of chemical pollutants.

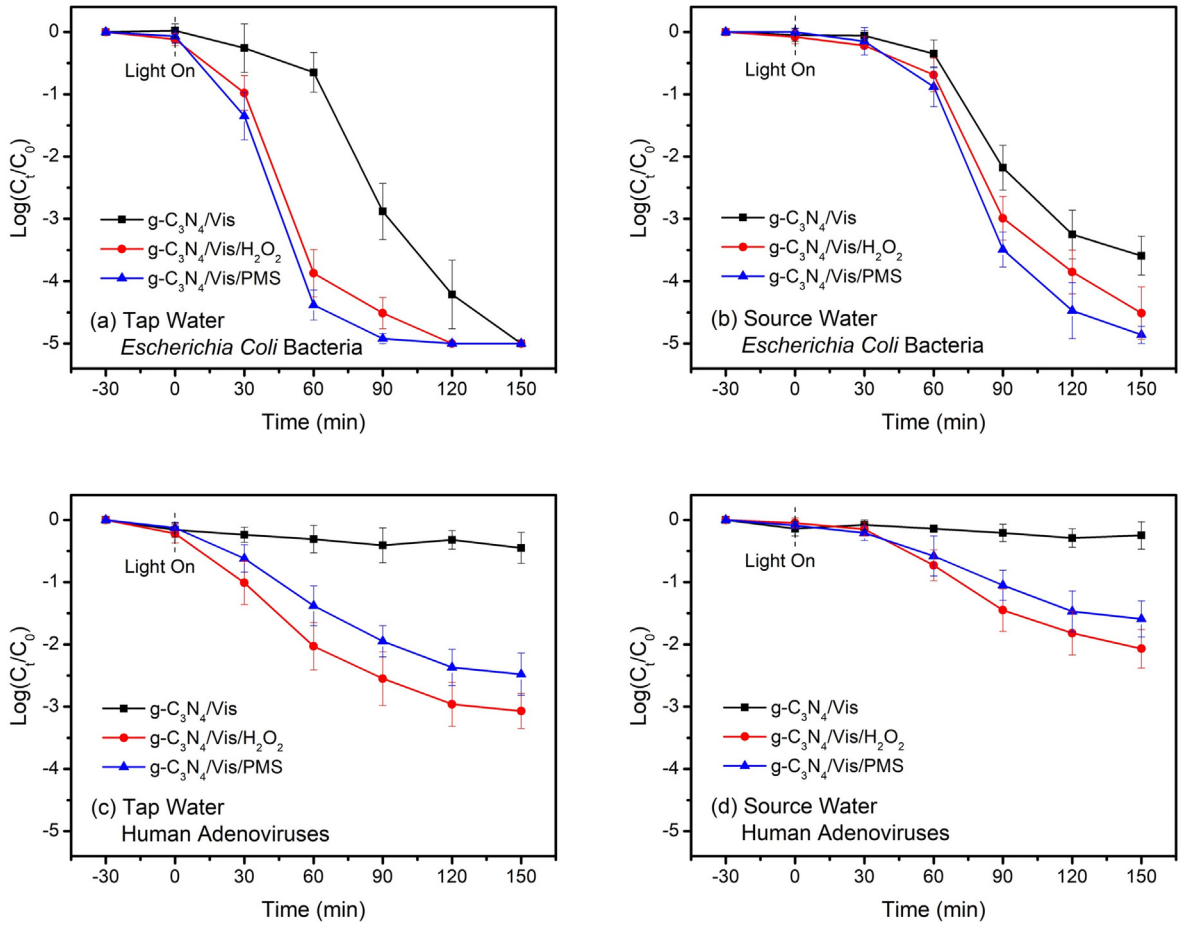

Fig. 8. Practical performance of g-C_3N_4-based metal-free visible-light-enabled photocatalytic disinfection: (a) *Escherichia coli* bacteria in tap water, (b) *Escherichia coli* bacteria in source water, (c) human adenoviruses in tap water, and (d) human adenoviruses in source water.

CRediT authorship contribution statement

Chi Zhang: Conceptualization, Methodology, Software, Validation, Formal analysis, Investigation, Resources, Data curation, Writing - original draft, Writing - review & editing, Visualization. **Yi Li:** Supervision, Project administration, Funding acquisition. **Chao Wang:** Writing - review & editing. **Xinyi Zheng:** Writing - review & editing.

Declaration of competing interest

The authors declare that they have no known competing financial interests or personal relationships that could have appeared to influence the work reported in this paper.

Acknowledgment

This study was supported by the National Key R&D Program of China (2019YFC0408301), the National Natural Science Foundation of China (51779076); the Fundamental Research Funds for the Central Universities (2019B05414); the Foundation for Innovative Research Groups of the National Natural Science Foundation of China (51421006); the Funds for Key Research and Development Project of Science and Technology Department of Jiangsu Province (BE2018738); the Six Talent Peaks Project in Jiangsu Province (2016-JNHB-007); the 333 Talent Project Foundation of Jiangsu Province and the Priority Academic Program Development of Jiangsu Higher Education Institutions (PAPD).

Appendix A. Supplementary data

Supplementary data to this article can be found online at https://doi.org/10.1016/j.scitotenv.2020.142588.

References

Baum, J., Pasvol, G., Carter, R., 2020. The R_0 journey: From 1950s malaria to COVID-19. Nature 582, 488.

Castro-Muñoz, R., 2019. Retention profile on the physicochemical properties of maize cooking by-product using a tight ultrafiltration membrane. Chem. Eng. Commun. 207, 887–895.

Castro-Muñoz, R., 2020. The role of new inorganic materials in composite membranes for water disinfection. Membranes 10, 101.

Castro-Muñoz, R., Yanez-Fernandez, J., Fila, V., 2016. Phenolic compounds recovered from agro-food by-products using membrane technologies: an overview. Food Chem. 213, 753–762.

Castro-Muñoz, R., Boczkaj, G., Gontarek, E., Cassano, A., Fíla, V., 2020. Membrane technologies assisting plant-based and agro-food by-products processing: a comprehensive review. Trends Food Sci. Technol. 95, 219–232.

Chen, J., Loeb, S., Kim, J.H., 2017. LED revolution: fundamentals and prospects for UV disinfection applications. Environ. Sci. Water Res. Technol. 3, 188–202.

Cui, Y.J., Ding, Z.X., Liu, P., Antonietti, M., Fu, X.Z., Wang, X.C., 2012. Metal-free activation of H_2O_2 by g-C_3N_4 under visible light irradiation for the degradation of organic pollutants. Phys. Chem. Chem. Phys. 14, 1455–1462.

Di Mascio, P., Martinez, G.R., Miyamoto, S., Ronsein, G.E., Medeiros, M.H.G., Cadet, J., 2019. Singlet molecular oxygen reactions with nucleic acids, lipids, and proteins. Chem. Rev. 119, 2043–2086.

Fenwick, A., 2006. Waterborne infectious diseases - could they be consigned to history? Science 313, 1077–1081.

Fernandez-Ibanez, P., Byrne, J.A., López, M.I.P., Singh, A., McMichael, S., Singhal, A., 2020. Photocatalytic Inactivation of Microorganisms in Water. Elsevier, Nanostructured Photocatalysts, pp. 229–248.
Gau, B.C., Chen, H., Zhang, Y., Gross, M.L., 2010. Sulfate radical anion as a new reagent for fast photochemical oxidation of proteins. Anal. Chem. 82, 7821–7827.
Gligorovski, S., Strekowski, R., Barbati, S., Vione, D., 2015. Environmental implications of hydroxyl radicals (•OH). Chem. Rev. 115, 13051–13092.
Huang, J.H., Ho, W.K., Wang, X.C., 2014. Metal-free disinfection effects induced by graphitic carbon nitride polymers under visible light illumination. Chem. Commun. 50, 4338–4340.
Krasner, S.W., Weinberg, H.S., Richardson, S.D., Pastor, S.J., Chinn, R., Sclimenti, M.J., et al., 2006. Occurrence of a new generation of disinfection byproducts. Environ. Sci. Technol. 40, 7175–7185.
Kumar, A., Raizada, P., Singh, P., Saini, R.V., Saini, A.K., Hosseini-Bandegharaei, A., 2020. Perspective and status of polymeric graphitic carbon nitride based Z-scheme photocatalytic systems for sustainable photocatalytic water purification. Chem. Eng. J. 391, 123496.
Leclerc, H., Schwartzbrod, L., Dei-Cas, E., 2002. Microbial agents associated with waterborne diseases. Crit. Rev. Microbiol. 28, 371–409.
Li, Y., Zhang, C., Shuai, D.M., Naraginti, S., Wang, D.W., Zhang, W.L., 2016. Visible-light-driven photocatalytic inactivation of MS2 by metal-free g-C_3N_4: Virucidal performance and mechanism. Water Res. 106, 249–258.
Li, C.M., Xu, Y., Tu, W.G., Chen, G., Xu, R., 2017a. Metal-free photocatalysts for various applications in energy conversion and environmental purification. Green Chem. 19, 882–899.
Li, G.Q., Wang, W.L., Huo, Z.Y., Lu, Y., Hu, H.Y., 2017b. Comparison of UV-LED and low pressure UV for water disinfection: Photoreactivation and dark repair of *Escherichia coli*. Water Res. 126, 134–143.
Liu, J., Liu, Y., Liu, N.Y., Han, Y.Z., Zhang, X., Huang, H., et al., 2015. Metal-free efficient photocatalyst for stable visible water splitting via a two-electron pathway. Science 347, 970–974.
Liu, C., Kong, D.S., Hsu, P.C., Yuan, H.T., Lee, H.W., Liu, Y.Y., et al., 2016. Rapid water disinfection using vertically aligned MoS_2 nanofilms and visible light. Nat. Nanotechnol. 11, 1098–1104.
Marugan, J., van Grieken, R., Pablos, C., Sordo, C., 2010. Analogies and differences between photocatalytic oxidation of chemicals and photocatalytic inactivation of microorganisms. Water Res. 44, 789–796.
Nosaka, Y., Nosaka, A.Y., 2017. Generation and detection of reactive oxygen species in photocatalysis. Chem. Rev. 117, 11302–11336.
Ong, W.J., Tan, L.L., Ng, Y.H., Yong, S.T., Chai, S.P., 2016. Graphitic carbon nitride (g-C_3N_4)-based photocatalysts for artificial photosynthesis and environmental remediation: are we a step closer to achieving sustainability? Chem. Rev. 116, 7159–7329.
Orooji, Y., Ghanbari, M., Amiri, O., Salavati-Niasari, M., 2020. Facile fabrication of silver iodide/graphitic carbon nitride nanocomposites by notable photo-catalytic performance through sunlight and antimicrobial activity. J. Hazard. Mater. 389, 122079.
Pichardo-Romero, D., Garcia-Arce, Z.P., Zavala-Ramírez, A., Castro-Muñoz, R., 2020. Current advances in biofouling mitigation in membranes for water treatment: an overview. Processes 8.
Płonka, I., Pieczykolan, B., 2020. Thermal methods, ultraviolet radiation, and ultrasonic waves for the treatment of waterborne pathogens. Waterborne Pathogens. Butterworth-Heinemann, pp. 143–167.
Rinas, A., Espino, J.A., Jones, L.M., 2016. An efficient quantitation strategy for hydroxyl radical-mediated protein footprinting using proteome discoverer. Anal. Bioanal. Chem. 408, 3021–3031.
Rodríguez-Chueca, J., Barahona-García, E., Blanco-Gutiérrez, V., Isidoro-García, L., 2020. Dos santos-García AJ. Magnetic $CoFe_2O_4$ ferrite for peroxymonosulfate activation for disinfection of wastewater. Chem. Eng. J. 125606.
Semenza, J.C., 2020. Cascading risks of waterborne diseases from climate change. Nat. Immunol. 21, 484–487.
Sun, P., Tyree, C., Huang, C.H., 2016. Inactivation of *Escherichia coli*, bacteriophage MS2, and *Bacillus* spores under UV/H_2O_2 and UV/peroxydisulfate advanced disinfection conditions. Environ. Sci. Technol. 50, 4448–4458.
Tao, Y.F., Ni, Q., Wei, M.Y., Xia, D.S., Li, X.X., Xu, A.H., 2015. Metal-free activation of peroxymonosulfate by g-C_3N_4 under visible light irradiation for the degradation of organic dyes. RSC Adv. 5, 44128–44136.
Thurston, J.H., Hunter, N.M., Wayment, L.J., Cornell, K.A., 2017. Urea-derived graphitic carbon nitride (u-g-C_3N_4) films with highly enhanced antimicrobial and sporicidal activity. J. Colloid Interface Sci. 505, 910–918.
Ursino, C., Castro-Muñoz, R., Drioli, E., Gzara, L., Albeirutty, M.H., Figoli, A., 2018. Progress of nanocomposite membranes for water treatment. Membranes 8, 18.
Wang, X.C., Maeda, K., Thomas, A., Takanabe, K., Xin, G., Carlsson, J.M., et al., 2009. A metal-free polymeric photocatalyst for hydrogen production from water under visible light. Nat. Mater. 8, 76–80.
Wang, W.J., Yu, J.C., Xia, D.H., Wong, P.K., Li, Y.C., 2013. Graphene and g-C_3N_4 nanosheets cowrapped elemental α-sulfur as a novel metal-free heterojunction photocatalyst for bacterial inactivation under visible-light. Environ. Sci. Technol. 47, 8724–8732.
Wang, H., Jiang, S.L., Chen, S.C., Li, D.D., Zhang, X.D., Shao, W., et al., 2016. Enhanced singlet oxygen generation in oxidized graphitic carbon nitride for organic synthesis. Adv. Mater. 28, 6940–6945.
Wang, L., Tong, J., Li, Y., 2019. River chief system (RCS): an experiment on cross-sectoral coordination of watershed governance. Front. Environ. Sci. Eng. 13.
Wordofa, D.N., Walker, S.L., Liu, H.Z., 2017. Sulfate radical-induced disinfection of pathogenic *Escherichia coli* O157:H7 via iron-activated persulfate. Environ. Sci. Technol. 4, 154–160.
World Health Organization, 2019. Drinking-water. Fact sheets. https://www.who.int/news-room/fact-sheets/detail/drinking-water.
Xia, P.F., Cao, S.W., Zhu, B.C., Liu, M.J., Shi, M.S., Yu, J.G., et al., 2020. Designing a 0D/2D S-scheme heterojunction over polymeric carbon nitride for visible-light photocatalytic inactivation of bacteria. Angew. Chem. Int. Ed. 59, 5218–5225.
Yadav, P., Nishanthi, S.T., Purohit, B., Shanavas, A., Kailasam, K., 2019. Metal-free visible light photocatalytic carbon nitride quantum dots as efficient antibacterial agents: an insight study. Carbon 152, 587–597.
Yan, S.C., Li, Z.S., Zou, Z.G., 2009. Photodegradation performance of g-C_3N_4 fabricated by directly heating melamine. Langmuir 25, 10397–10401.
Zhang, C., Li, Y., Shuai, D.M., Zhang, W.L., Niu, L.H., Wang, L.F., et al., 2018a. Visible-light-driven, water-surface-floating antimicrobials developed it from graphitic carbon nitride and expanded perlite for water disinfection. Chemosphere 208, 84–92.
Zhang, C., Li, Y., Zhang, W.L., Wang, P.F., Wang, C., 2018b. Metal-free virucidal effects induced by g-C_3N_4 under visible light irradiation: statistical analysis and parameter optimization. Chemosphere 195, 551–558.
Zhang, C., Li, Y., Shuai, D.M., Shen, Y., Wang, D.W., 2019a. Progress and challenges in photocatalytic disinfection of waterborne viruses: a review to fill current knowledge gaps. Chem. Eng. J. 355, 399–415.
Zhang, C., Li, Y., Shuai, D.M., Shen, Y., Xiong, W., Wang, L.Q., 2019b. Graphitic carbon nitride (g-C_3N_4)-based photocatalysts for water disinfection and microbial control: a review. Chemosphere 214, 462–479.
Zhang, C., Zhang, M.Y., Li, Y., Shuai, D.M., 2019c. Visible-light-driven photocatalytic disinfection of human adenovirus by a novel heterostructure of oxygen-doped graphitic carbon nitride and hydrothermal carbonation carbon. Appl. Catal. B Environ. 248, 11–21.
Zhang, C., Li, Y., Li, J., 2020. Improved disinfection performance towards human adenoviruses using an efficient metal-free heterojunction in a vis-LED photocatalytic membrane reactor: operation analysis and optimization. Chem. Eng. J. 392, 123687.
Zhao, H.X., Yu, H.T., Quan, X., Chen, S., Zhang, Y.B., Zhao, H.M., et al., 2014. Fabrication of atomic single layer graphitic-C_3N_4 and its high performance of photocatalytic disinfection under visible light irradiation. Appl. Catal. B Environ. 152, 46–50.